Journal of Molecular Catalysis A: Chemical 356 (2012) 121–127

Contents lists available at SciVerse ScienceDirect

Journal of Molecular Catalysis A: Chemical

journal homepage: www.elsevier.com/locate/molcata

Promotional effect of CeO_X for NO reduction over V_2O_5/TiO_2-carbon nanotube composites

Qian Li [a], Xiaoxu Hou [b], Hangsheng Yang [a,*], Zhaoxia Ma [a], Junwei Zheng [a], Fu Liu [a], Xiaobin Zhang [a], Zhongyong Yuan [b]

[a] State Key Laboratory of Silicon Materials, Department of Materials Science and Engineering, Zhejiang University, Zheda Road 38, Hangzhou 310027, China
[b] Institute of New Catalytic Materials Science, Key Laboratory of Advanced Energy Materials Chemistry (Ministry of Education), College of Chemistry, Nankai University, Tianjin 300071, China

ARTICLE INFO

Article history:
Received 30 October 2011
Received in revised form 4 January 2012
Accepted 4 January 2012
Available online 13 January 2012

Keywords:
NO_X
SCR
V_2O_5
CeO_2
CNT

ABSTRACT

A series of V_2O_5–CeO_X/TiO_2-carbon nanotube composites were prepared by sol–gel method and their catalytic activity for the reduction of NO_X with NH_3 was compared. $V_2O_5CeO_X/TiO_2$ (Ce/V = 9) achieved a NO_X removal efficiency of 92% and 98% at 200 °C and 250 °C, respectively. SEM, XRD, XPS, BET, Raman, TPD and TPR were employed to probe the promotional effect of CeO_X. The appearance of Ce^{3+} is found to increase chemisorbed oxygen thus facilitates the catalytic reduction of NO_X. The poisoning effect caused by SO_2 was found to depend on temperatures and gas velocity strongly. Moreover, the existence of excess oxygen was found to be essential (2% of O_2 compared to 500 ppm NO_X) to keep high SCR activity.

1. Introduction

Nitrogen oxides (NO_X) discharged from power plants, waste incinerators, industrial boilers, engines, and automobiles can result in acid rain, photochemical smog, and ozone depletion. These detrimental effects to the environment have aroused worldwide attention. Many approaches have been investigated to reduce NO_X emission. Among them, selective catalytic reduction (SCR) technique has been proven to be one of the most effective methods for reducing NO_X emissions [1,2]. A large number of SCR catalysts have been explored, including noble metals [3,4], transition metal oxides [5,6] and zeolites [7,8]. Especially, V_2O_5–WO_3/TiO_2 based catalysts have been extensively used in the industry. However, the operating temperature for these catalysts is usually above 300 °C, and the exhaust gases usually contain a large number of fly ash and SO_2, which can easily deactivate the catalysts. Thus, the development of active SCR catalysts that can be operated at relatively low temperatures (below 250 °C) is needed, so that SCR systems could be installed downstream of the desulfurizer and electrostatic precipitator, where the flue gas temperature is relatively low (below 250 °C). Low-temperature catalysts can also contribute to lower energy consumption and help simplify the retrofitting of SCR devices for flue gas cleaning [9].

A series of catalysts, including V_2O_5/AC [10], V_2O_5/CNTs [11], Mn–Ce/TiO_2 [12], V_2O_5–MnO_X/TiO_2CNTs [13] have been reported to present high activity at relatively low temperatures. Researchers have tried to introduce metal oxides to traditional V_2O_5–TiO_2 and MnO_X–CeO_2 catalysts to further improve NO_X removal efficiency at low temperatures. Amiridis et al. [14] screened the effect of introducing metal oxides to V_2O_5/TiO_2 and found that WO_3 and MoO_3 exhibit the most significant promotion of the catalyst, whereas MnO_2, Ga_2O_3, La_2O_3, SnO_2, and ZnO appear to poison the catalyst. Phil et al. [15] reported that Se-, Sb-, Cu-, and S-doped V_2O_5/TiO_2 catalysts show high catalytic activity for NH_3-SCR of NO_X at temperatures between 150 and 400 °C. Recently, CeO_2 attracted researchers' interest due to its special structure and property. CeO_2 has fluorite-structure and could store and release oxygen via the redox shift between Ce^{4+} and Ce^{3+} under oxidizing and reducing conditions, respectively [16–18]. CeO_X can also be utilized as catalyst support, promoter or even active species. Qi and Yang [19] achieved good catalytic performance in reduction of NO_X over catalyst MnO_X–CeO_2. Chen [18] and Wu et al. [20,21] improved SCR performance for V_2O_5–WO_3/TiO_2 and MnO_X/TiO_2, using CeO_X as promoter, respectively. Moreover, CeO_X has been used as structure promoter and a buffer in redox cycle to enhance catalytic property of catalyst Pd/Al [16]. And CeO_2-zeolite was reported to be very active for reduction of NO with NH_3 [22].

* Corresponding author. Tel.: +86 571 87951404; fax: +86 571 87951404.
E-mail address: hsyang@zju.edu.cn (H. Yang).

1381-1169/$ – see front matter © 2012 Elsevier B.V. All rights reserved.
doi:10.1016/j.molcata.2012.01.004

Recently, we found that SCR activity of the traditional V_2O_5/TiO_2 catalyst was significantly promoted by the introduction of CNTs [23]. In the present study, CeO_X was added into catalyst V_2O_5/TiO_2-CNTs trying to further improve SCR activity for NO_X removal. Also, the influences of oxygen, SO_2 and gas velocity on catalyst V_2O_5–CeO_X/TiO_2-CNTs were examined with respect of its application in large scale.

2. Experimental method

2.1. Catalyst preparation

Samples were prepared by sol–gel method. The multi-walled CNTs (MWCNTs) purchased from Shenzhen Nanoport Co. Ltd. were purified in concentrated nitric acid for 2 h and then dried and ground for later use. Tetrabutyl titanate, ammonium metavanadate, chromic nitrate, cobalt nitrate, cerium nitrate, nickel nitrate and ammonium molybdate were used as precursors of TiO_2, V_2O_5, Cr_2O_3, Co_3O_4, CeO_2, NiO and MoO_3, respectively.

Details of catalyst synthesis are as follows. First, purified MWCNTs, acetic acid and tetrabutyl titanate were ultrasonically dispersed in ethanol for 30 min, ammonium metavanadate dissolved in oxalic acid, chromic nitrate (cobalt nitrate, cerium nitrate, nickel nitrate and ammonium molybdate) and deionized water were added to above suspension and then ultrasonicated until a sol was formed. The sol was aged in air until it transformed into a gel. The gel was dried at 100 °C and finally calcined at 450 °C for 2 h in N_2 to obtain V_2O_5–MO_X/TiO_2-CNTs (M: Cr, Co, Ce, Ni, Mo). The catalysts are denoted as VM_XTiC, where X represents nominal atomic ratio of M to V. V_2O_5/TiO_2-CNTs catalyst was also prepared through the same method for comparison. The physicochemical properties of the catalysts are summarized in Table 1.

2.2. Catalyst characterization

X-ray diffraction (XRD) patterns were recorded on an X-ray diffractometer (Philips XD-98) using Cu K_α radiation (λ = 0.15406 nm). Brunauer–Emmett–Teller surface areas, pore diameter, and pore volume were measured using an ASAP2000 physical adsorber. Sample morphology and dispersion were characterized by scanning electron microscopy (SEM; Hitachi S-4800). Element analysis of catalysts was done by X-ray photoelectron spectroscopy (XPS), using a Kratos Axis Ultra-DLD. The Raman spectra were obtained on a Labor Raman HR-800 (JDbin Yvon) at 10 mW of the 514.5 nm line of an Ar ion laser to analyze the surface species and the interaction among the metal oxides.

The temperature-programmed reduction (H_2-TPR) experiment was carried out from 50 to 800 °C in a 1690 Gas Chromatograph using 50 mg samples of the catalysts. Prior to the analysis, the catalysts were pretreated at 300 °C for 30 min in air. The TPR runs were carried out at a heating rate of 10 °C min^{-1} using a stream of 5% H_2 in argon at a flow rate of 40 mL min^{-1}. The hydrogen consumption was measured by a thermal conductivity detector calibrated with CuO.

The NH_3 temperature-programmed desorption (NH_3-TPD) experiment was performed to determine the acidity of catalysts. A 30 mg sample of each catalyst was loaded in the reactor and was pretreated in a helium stream (30 mL min^{-1}) at 550 °C for 1 h, and then cooled to 100 °C in the same stream. The pretreated sample was then exposed to NH_3 (4%) at a flow rate of 20 mL min^{-1} for 3 h. The physisorbed NH_3 was removed by flushing the catalysts with N_2 at a flow rate of 30 mL min^{-1} for 1 h before starting the TPD experiment. Experimental runs were recorded by heating the samples in N_2 (30 mL min^{-1}) from 100 to 600 °C at a heating rate of 10 °C min^{-1}.

2.3. Catalytic activity characterization

All catalysts were pasted to 10 aluminum plates (3 cm × 10 cm) with 20% organoclay, which were then inserted into a fixed-bed flow reactor. The distance between each plate was approximately 5 mm. An NO–NO_2–NO_X analyzer (Testo AG-testo 350) was used to measure the inlet and outlet concentrations of NO and NO_2. The catalyst temperature was measured using a thermocouple projecting into the center of the reactor. Dry air was used as the source of O_2, and N_2 was used as the balance gas. The premixed gases (1% NO/Ar, 1% NH_3/Ar) were prepared to formulate the flue gas in the experiments. The reaction conditions were as follows: 500 ppm NO, 500 ppm NH_3, 6% O_2, 200 ppm SO_2 (when used). The reacting gases were mixed and preheated at 100 °C before being introduced into the reactor. The activity measurements were performed from 100 to 300 °C, at increments of 25 °C under varied GHSV of 7500–30,000 h^{-1}.

3. Results and discussion

3.1. Catalytic activity

3.1.1. Effect of different dopant on activity of V_2O_5/TiO_2-CNTs

As shown in Fig. 1(a), no great effect was observed on the catalytic property of catalyst VTiC with addition of Ni, Cr and Mo, at temperature between 100 and 300 °C, and the Co even had a negative influence on NO_X reduction. Fortunately, catalytic improvement took place with the addition of CeO_X to VTiC and the reactivity was further improved by increasing the CeO_X content (Ni, Cr, Mo, Co and Ce were introduced with the same atomic ratio (M/V = 1, M: Ni, Cr, Mo, Co, Ce)). The NO_X conversion increased dramatically to 92% at 200 °C over catalyst VCe_9TiC upgraded by CeO_X. To better evaluate catalytic activity for NO_X conversion, kinetic parameters were calculated according to Eqs. (1) and (2), which were based on the assumption that the reaction is first-order dependent on NO_X and zero-order dependent on NH_3 [24,25].

$$k = -\frac{V}{W} \times \ln(1 - x) \quad (1)$$

$$k = A \ \exp\left(\frac{E_a}{RT}\right) \quad (2)$$

where k is the reaction rate coefficient (mL g^{-1} s^{-1}), V is the total gas flow rate (mL s^{-1}), W is the mass of the catalyst (g), x is

Table 1
Summary of the surface element composition and structure property of catalysts.

Catalysts	Atomic ratio (V, Ce, Ti, V/Ce, V/Ti)[a]	S (m^2/g)	Pore volume (cm^3/g)	Pore diameter (nm)
VTiC	(0.0015, –, 0.1194, –, 1:80)	109	0.25	8.1
VCe_3TiC	(0.0015, 0.0068, 0.1015, 1:4.5, 1:67)	126	0.23	6.4
VCe_6TiC	(0.0017, 0.0132, 0.0877, 1:7.8, 1:52)	120	0.17	5.0
VCe_9TiC	(0.0015, 0.0243, 0.0962, 1:16, 1:64)	133	0.19	5.0

[a] The atomic ratio of the composition is determined by XPS. Moreover, the CNTs concentration was approximately 10% in each catalyst.

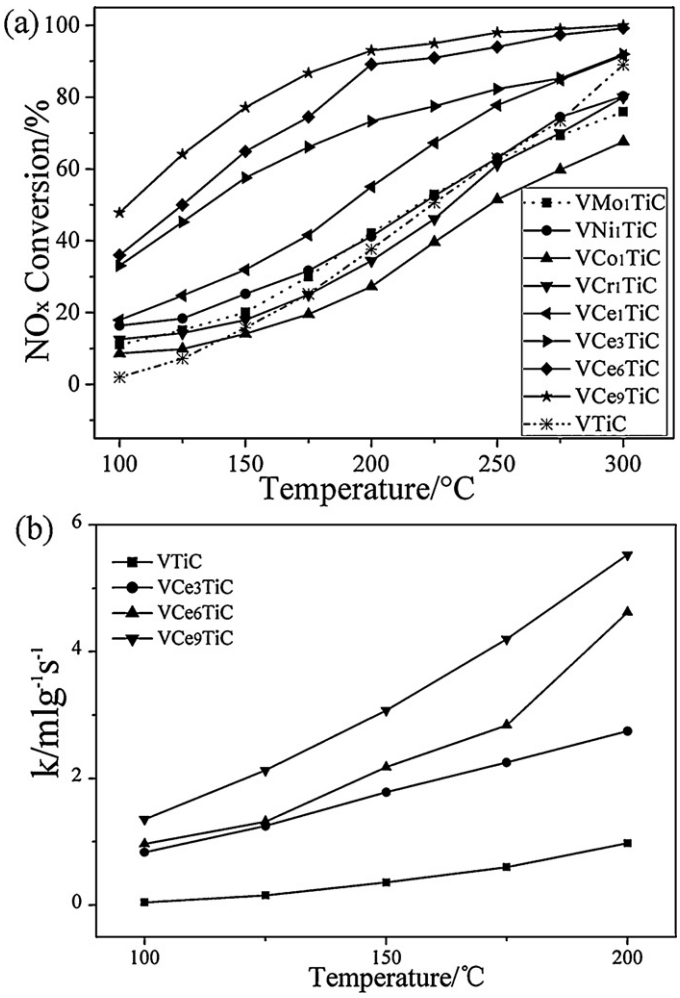

Fig. 1. (a) NO_X conversion at temperatures over different catalysts. (b) The kinetic rate constant k at temperatures over different catalysts. Reaction conditions: NO 500 ppm, NH_3 500 ppm, O_2 6%, N_2 as the balance gas, GHSV = 7500 h^{-1}.

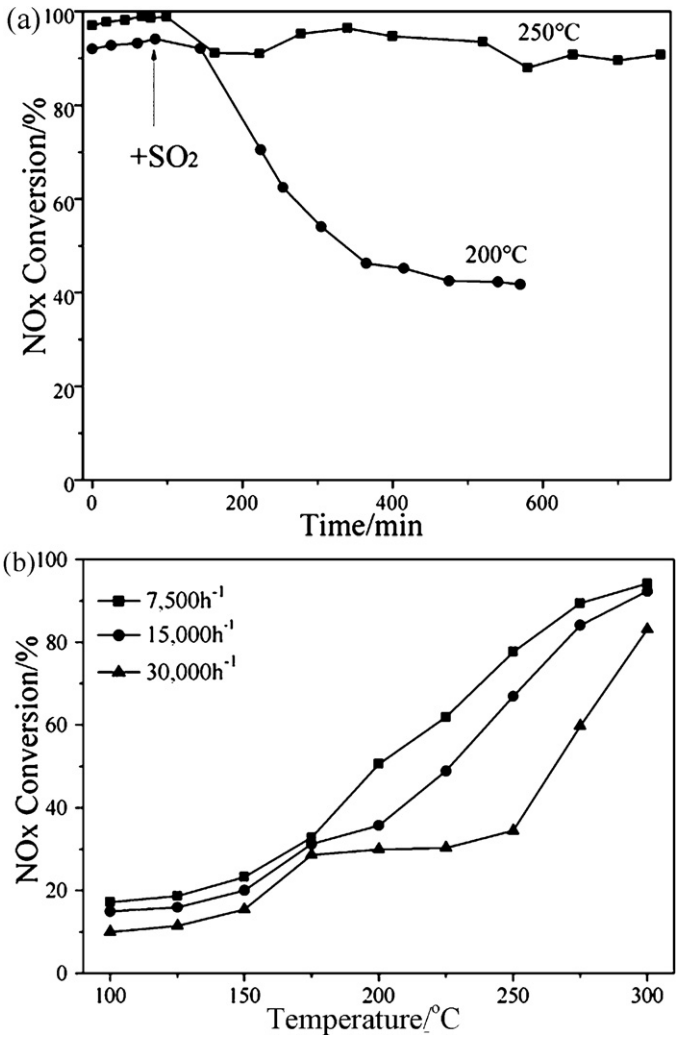

Fig. 2. (a) Catalytic reduction of NO_X at different temperatures over catalyst VCe_9TiC with SO_2. Reaction conditions: NO 500 ppm, NH_3 500 ppm, O_2 6%, SO_2 200 ppm (when used), N_2 as the balance gas, GHSV = 7500 h^{-1}. (b) Catalytic reduction of NO_X over catalyst VCe_9TiC under varied GHSV. Reaction conditions: NO 500 ppm, NH_3 500 ppm, O_2 6%, 200 ppm SO_2, N_2 as the balance gas.

the conversion of NO_X (%), E_a is the apparent activation energy (J mol^{-1}), A is the pre-exponential factor, R is the gas constant (8.3145 J mol^{-1} K^{-1}), and T is the temperature (K).

The variation of k with temperatures is presented in Fig. 1(b). The values of k for the catalysts VTiC and VCe_9TiC were found to be 1.0 and 5.5 at 200 °C respectively, which indicates a marked promotion in the reaction rate with the introduction of CeO_X to VTiC. The apparent activation energy for catalysis by VTiC, VCe_9TiC was calculated to be 32.95 and 18.9 kJ mol^{-1} respectively, according to the Arrhenius plot. These calculations indicate that catalytic reaction was easier over VCe_9TiC than VTiC.

3.1.2. Effect of SO_2 on reduction of NO_X over catalyst VCe_9TiC

SO_2 is a common component of industrial exhaust gas, thus it is important to investigate its influence on SCR activity. The catalytic performances with introduction of SO_2 to flue gas over catalyst VCe_9TiC are presented in Fig. 2. Fig. 2(a) shows experimental results of the time-dependent SO_2 resistance at 200 °C and 250 °C, respectively. Slight decrease of catalytic activity upon addition of SO_2 was observed at 250 °C while the catalyst VCe_9TiC can still reach 90% NO_X conversion even after 11 h. To contrast, the NO_X conversion decreased from 93% to 41% within 8 h upon the introduction of SO_2 at 200 °C. Evidently the poison effect brought by SO_2 depends on the reaction temperature greatly, which was consistent with Goo et al.'s report [24]. According to previous study [26], the balance of sulfate salt formation and consumption is the main mechanism that controls the deactivation of the catalyst. The deposition rate of sulfate is determined by the difference between its formation and reaction with NO_X. At lower temperature, the deposition rate outweighs the consumption rate of sulfate species thus the sulfate species may deposit on the surface of catalyst and cover the active site, which results in the poison of catalyst. As shown in Fig. 2(b), catalytic reactivity of VCe_9TiC as a function of temperatures under different gas velocity was examined. On the one hand, the contact time between catalyst and NO_X molecular reduced with high GHSV. On the other hand, high gas velocity increased the sulfate deposition, which caused an over deposition of sulfate species. These two effects combined to explain the reduction of catalytic activity over catalyst VCe_9TiC under high gas velocity.

3.1.3. Effect of O_2 on catalytic performance over catalyst VCe_9TiC

O_2 is very essential for the selective catalytic reaction [27]. Accordingly, the effect of O_2 concentration was also performed in the present study and the results are displayed in Fig. 3. As shown in Fig. 3(a), catalytic performance was suppressed greatly with O_2 concentration of 0.09% while can recover to 77% quickly with introduction of 2% O_2 at 175 °C. However, no great increase of catalytic property was observed when the O_2 concentration exceeds 3%,

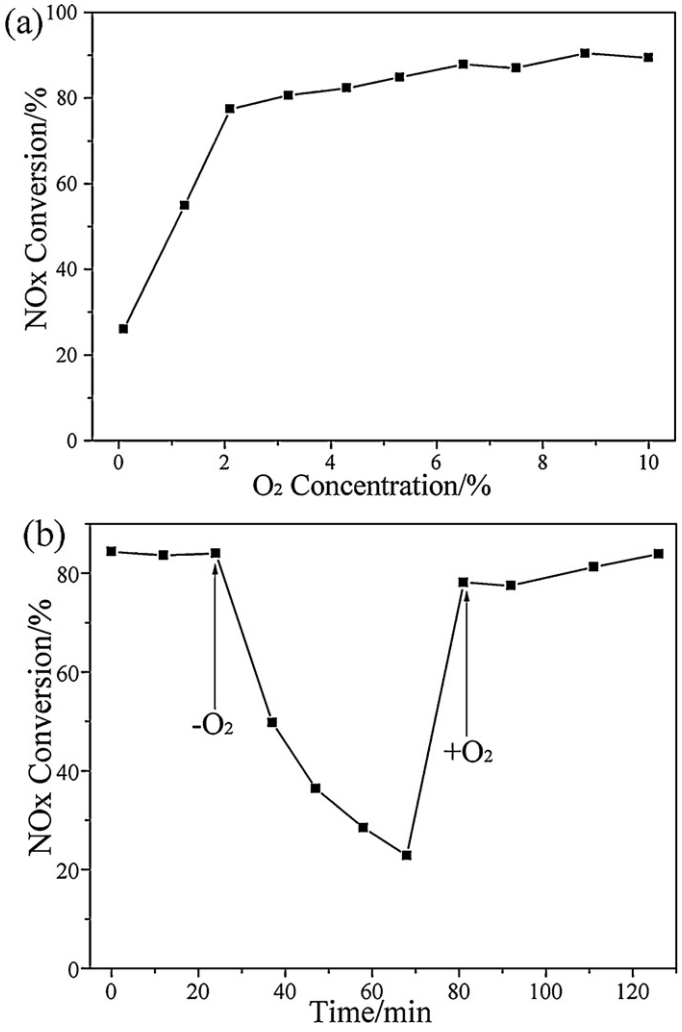

Fig. 3. (a) Effect of O_2 concentration on catalytic performance over VCe_9TiC at 175 °C. (b) Transient response over catalyst VCe_9TiC upon switching off and on O_2 at 175 °C. Reaction conditions: NO 500 ppm, NH_3 500 ppm, O_2 0–10%, N_2 as the balance gas, GHSV = 7500 h^{-1}.

which was consistent with other reports [19,27]. The significance of O_2 concentration can also be verified by another transient experiment presented in Fig. 3(b). The catalytic activity decreased quickly upon turning off O_2 and recovered to original level with switching on O_2 again. These observations indicated the importance of O_2 concentration to SCR reaction especially under low oxygen concentration and that lattice oxygen participated in the reduction of NO_X when O_2 was shut off.

3.2. Catalyst characterization

3.2.1. Microstructure and morphology analysis

Fig. 4(a)–(d) shows the SEM images of the catalysts VTiC, VCe_3TiC, VCe_6TiC and VCe_9TiC. The catalyst particles were dispersedly coated on the surfaces of the CNTs with uniform distribution. Vanadium dispersion was investigated by EDX-mapping as shown in Fig. 4(e)–(h). With the introduction of CeO_X, the aggregation of V_2O_5 was further reduced.

The XRD patterns of VTiC, VCe_3TiC, VCe_6TiC and VCe_9TiC are shown in Fig. 5. The peaks corresponding to TiO_2 (anatase PDF# 21-1272) appeared in the patterns of all catalysts. The peak at 26.4° is attributed to the peak for CNTs that overlapped with that of TiO_2 at 25.3° [28]. The peak located at 30.8° was assigned to titanium oxide (PDF# 65-2448) over catalyst VTiC. No peak corresponding

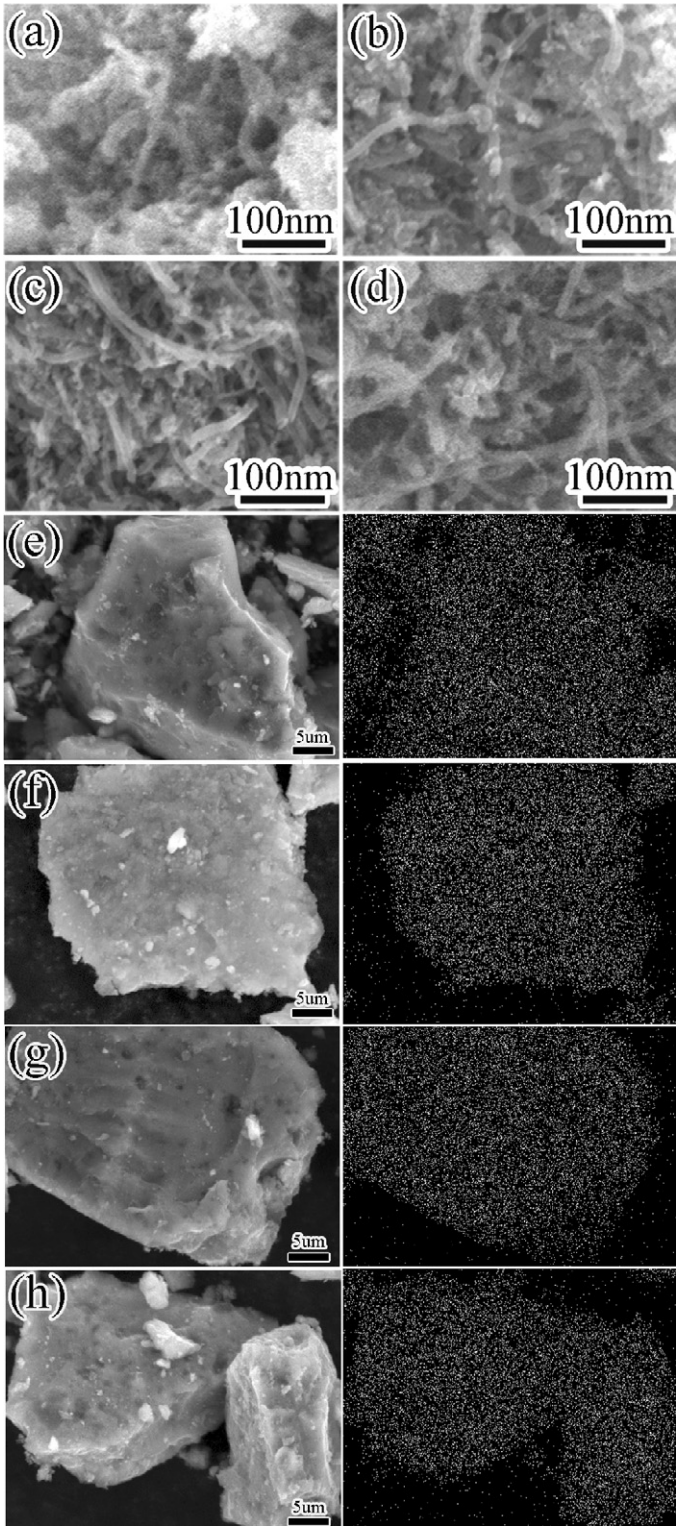

Fig. 4. SEM images (a–d) and V_k-EDX mapping patterns (e–h) for catalysts VTiC, VCe_3TiC, VCe_6TiC, VCe_9TiC, respectively.

to CeO_X and V_2O_5 was observed in all catalysts; which indicates that the amount of its crystalline was too small to be detected. Moreover, the peaks of VTiC were much sharper than those of the other catalysts. This indicates that the grain size of the catalysts decreased with the addition of CeO_X. The crystalline sizes of VTiC, VCe_3TiC, VCe_6TiC, and VCe_9TiC calculated from the XRD peaks at 26.4° were 8.5, 4.9, 4.6, and 3.6 nm, respectively. The addition of

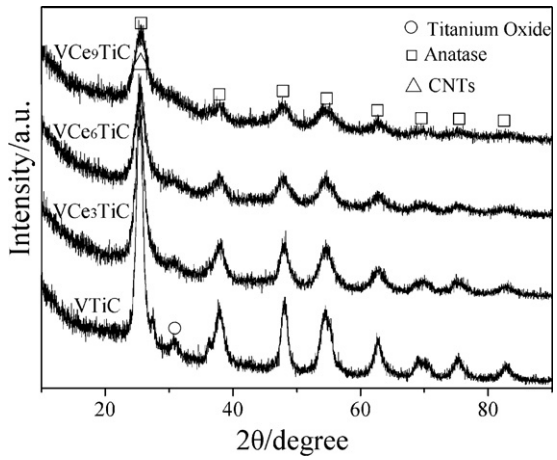

Fig. 5. XRD patterns of catalysts with CeO_X.

CeO_X might hinder the sinter and aggregation of nano particles, which was in line with Fig. 4 and other report [16]. Moreover, the intensity of peaks corresponding to TiO_2 reduced with the addition of CeO_X, though no peaks assigned to CeO_X appeared. In summary, the introduction of CeO_X hindered aggregation of nano particles, which contributed to good dispersion of V_2O_5.

The specific surface area, pore volume, and pore size of the catalysts are summarized in Table 1. Surface area increased while the pore volume and pore diameter both decreased with the introduction of CeO_X. Although the surface area of the catalysts may not be the determining parameter in SCR activity [29], the high surface area can promote the catalytic reduction of NO_X by NH_3, since high surface area can offer more active sites for reaction.

The V_2O_5 contents of the surfaces of VTiC, VCe_3TiC, VCe_6TiC, and VCe_9TiC were 0.48, 0.41, 0.43 and 0.39 $\mu mol\,m^{-2}$, respectively (assuming that all active components were present on the surface of the catalysts). The surface V_2O_5 contents are lower than value obtained by monolayer coverage (commonly accepted to be 6–7 $\mu mol\,m^{-2}$ for vanadia) [11].

3.2.2. Surface species analysis

The Raman spectra of the catalysts VTiC, VCe_3TiC, VCe_6TiC, and VCe_9TiC are shown in Fig. 6. Typical Raman peaks of CNTs centered at 1350 (D peak), 1590 cm^{-1} (G peak) and 2700 cm^{-1} in the spectra of all catalysts were detected [30]. Catalysts VTiC and VCe_3TiC showed Raman peaks at 144, 196, 395, 511, and 633 cm^{-1}, which correspond to the anatase phase of TiO_2 [31]. The intensity of the anatase peaks decreased with the introduction of CeO_X so that

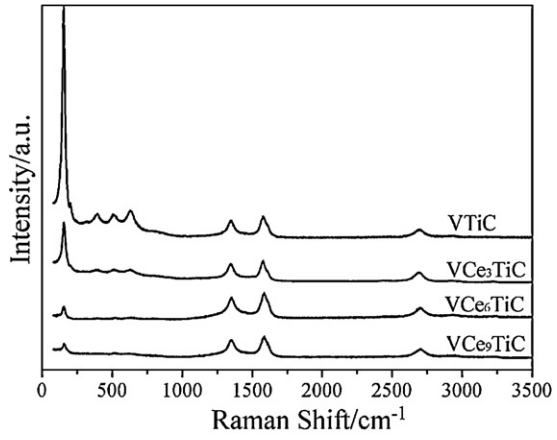

Fig. 6. Raman spectra of catalysts with CeO_X.

Table 2
NH_3-TPD results over catalysts with different CeO_X content.

Catalysts	n_{NH_3} ($\mu mol\,g^{-1}$)			
	240 °C (L)	380 °C (H)	Total	I_H/I_{H+L}
VTiC	40	14	54	0.26
VCe_3TiC	40	22	62	0.35
VCe_6TiC	25	12	37	0.32
VCe_9TiC	34	29	63	0.46

only peak centered at 144 cm^{-1} appeared on catalysts VCe_6TiC, and VCe_9TiC, which was in line with results of XRD. Moreover, no Raman peak ascribed to V_2O_5 and CeO_X was observed on all catalyst spectra, which may be due to the low V_2O_5 loading on the surface or the interaction of V, Ce, Ti and C [17,31].

The XPS spectra of O1s peaks are displayed in Fig. 7(a). The peak at 529.6–530.0 eV corresponds to lattice oxygen (hereafter denoted as O_β), whereas the peak at 531.3–531.7 eV corresponds to several O1 s states of surface-adsorbed oxygen (hereafter denoted as O_α) [32]. As shown in Fig. 7(a), the O_β concentration decreased with the addition of CeO_X. The relative concentration ratio of $O_\alpha/(O_\alpha + O_\beta)$ of VTiC and VCe_6TiC was calculated to be 0.21and 0.29, respectively. The concentration of chemisorbed oxygen increased with the addition of CeO_X, which was suggested to be helpful for SCR reaction [18,32]. And the ease of formation of labile oxygen vacancies and particularly the relatively high mobility of bulk oxygen species of CeO_X may contribute to the improvement of chemisorbed oxygen [17].

V2p peaks for catalysts are presented in Fig. 7(b). V^{5+} (517.4 eV), V^{4+} (516.2 eV) and V^{3+} (515.1 eV) ion [33] all appeared on catalyst VTiC and the intensity of V^{3+} declined gradually with the addition of CeO_X. In addition, the V2p peaks shifted to higher binding energy when CeO_X was introduced, indicating quantivalency of V species increased thus the V^{3+} reduced. The shortened red-ox cycle of V^{5+}/V^{4+} perhaps favors the catalytic reaction as Zhong and Li [34] thought the formation of V^{4+} facilitated to the SCR reaction.

XPS spectra of Ce3d for catalysts are displayed in Fig. 7(c). The peaks labeled u are due to $3d_{3/2}$ spin–orbit states, and those labeled v are the corresponding $3d_{5/2}$ states [17]. The bands labeled u1 and v1 represent the $3d^{10}4f^1$ initial electronic state, corresponding to Ce^{3+}, whereas the peaks labeled u, u2, u3, v, v2, and v3 represent the$3d^{10}4f^0$ state of Ce^{4+} ions [18]. The Ce^{3+} ions were predominant for all catalysts and a small fraction of Ce^{4+} ions appeared with high Ce/V ratio. It demonstrated that Ce mainly existed in the form of Ce^{3+} for catalyst VCe_9TiC. It was reported [18,27,35] that Ce^{3+} could create a charge imbalance, the vacancies and unsaturated chemical bonds on the catalyst surface thus facilitated the formation of chemisorbed oxygen, so a large number of Ce^{3+} ions will contribute to the improved catalytic property.

Fig. 7(d) shows the XPS spectra of Ti2p for catalysts VTiC, VCe_6TiC and VCe_9TiC. No great change can be drawn from the comparison of the XPS patterns, which indicated that the introduction of CeO_X did not influence the structure of TiO_2 support. No solid solution was observed for our study, which was consistent with the results of XRD and Raman.

3.2.3. Surface acidity

Fig. 8 shows the deconvolution of NH_3-TPD profiles over catalysts VTiC, VCe_3TiC, VCe_6TiC and VCe_9TiC. Two peaks centered at about 240 °C (L), 380 °C (H) were deconvoluted on all profiles. The quantity analysis of acidic sites over catalysts with different CeO_X content is summarized in Table 2. The total amount of acid sites increased with addition of CeO_X except for catalyst VCe_6TiC. However, the ratio of strong acid and total acid content denoted as I_H/I_{H+L} increased remarkably upon the introduction of CeO_X. This clearly indicated that CeO_X could increase acidity of

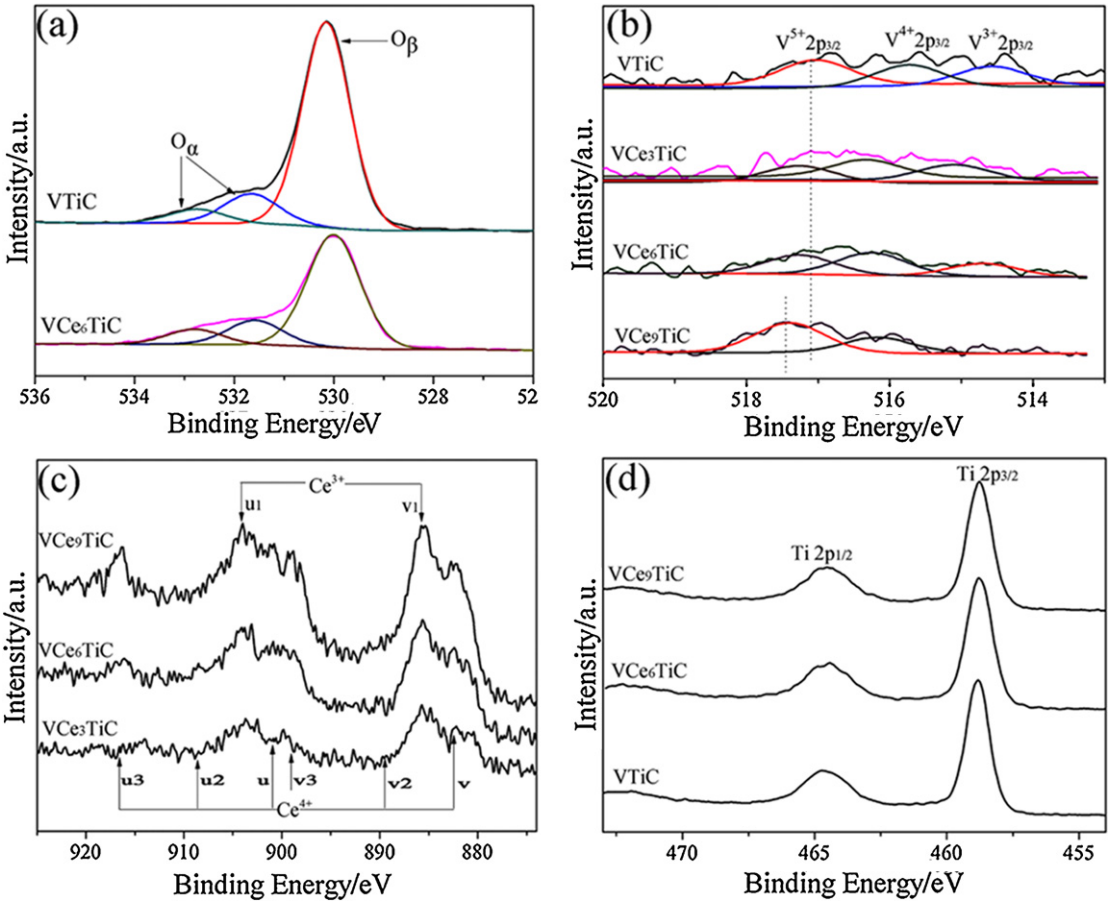

Fig. 7. XPS spectra over catalysts with CeO_X. (a): O1 s; (b): V2p; (c): Ce3d; (d): Ti2p.

upgraded catalysts especially for improving strong acid thus facilitates the adsorption and activation of NH_3 during catalytic reaction. Based on the foregoing analysis, it seems that the enhanced acidity contributes to promotion of NH_3 adsorption and activation thus enhanced the catalytic activity in NH_3–deNO_X [23,36].

3.2.4. Reducibility

Fig. 9 presents the H_2-TPR profiles of VTiC, VCe_3TiC and VCe_9TiC. A broad peak centered at 550 °C was detected over VTiC, which could be assigned to the reduction of vanadia from V^{5+} to V^{3+} and V^{4+} to V^{3+} [37]. Catalysts VCe_3TiC and VCe_9TiC both gave rise to one broad peak (380–800 °C), which could be ascribed to overlap of reduction of Ce^{4+} to Ce^{3+}, V^{5+} to V^{3+} and V^{4+} to V^{3+} [18,37,38]. In contrast to a previous report that several peaks above 627 °C were observed on unsupported V_2O_5 [37], only one peak was observed in our study, which was associated with good dispersion of V_2O_5 on the support. Note that, the H_2 consumption peaks over doped catalysts were broadened and the reaction started at relatively low temperatures with introduction of CeO_X. Moreover, H_2 consumption of VTiC, VCe_3TiC and VCe_9TiC was calculated to be 302, 688 and 832 μmol g^{-1}, respectively. A large increase in H_2 consumption was observed upon the addition of CeO_X, which probably resulted from

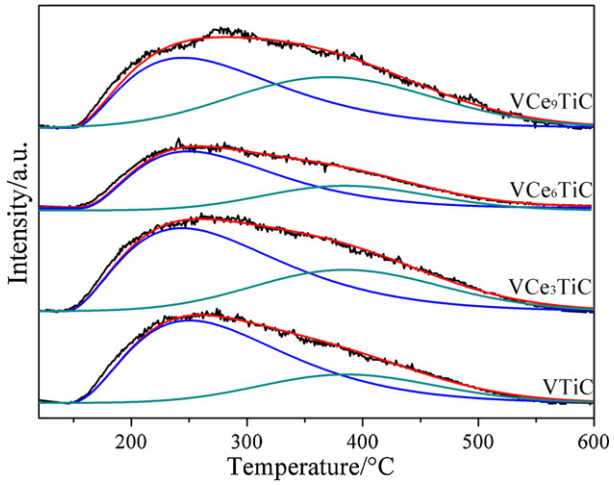

Fig. 8. Typical NH_3-TPD curves of CeO_X contained catalysts.

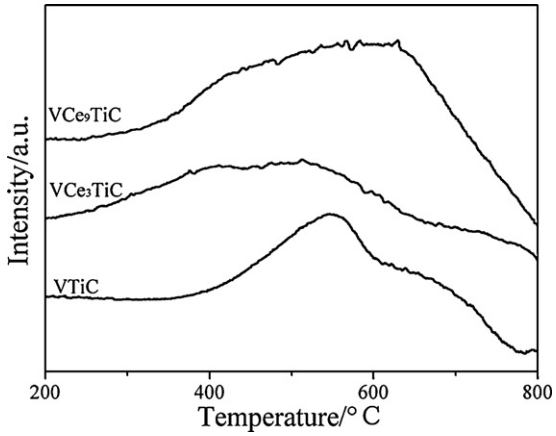

Fig. 9. Typical H_2-TPR curves of CeO_X contained catalysts.

the large number of chemisorbed oxygen introduced by CeO_X as shown in Fig. 7a.These observations indicate that the reducibility of upgraded catalysts is improved upon the addition of CeO_X, which could contribute to NH_3-SCR activity [13].

4. Conclusion

Co, Ce, Cr, Mo, Ni were introduced to catalyst V_2O_5/TiO_2-CNTs with sol–gel method and Ce was proved to be most effective to promote NH_3-SCR activity. A large number of Ce^{3+} contributes to the increase of chemisorbed oxygen, which favors the SCR activity. The aggregation of catalyst might be inhibited by CeO_X thus result to the increase of specific surface. Moreover, the increase of surface acidity and reducibility both contribute to the extra NO_X conversion upon addition of CeO_X. The deactivation of catalyst VCe_9TiC caused by SO_2 depends on reaction temperatures and gas velocity strongly. And at least 2% of oxygen in exhaust gas is essential to keep high SCR activity.

Acknowledgments

This work was supported by the Environmentally Sustainable Management of Medical Wastes in China (Contract No. C/V/S/10/251), the National Natural Foundation of Zhejiang Province, China (Grant No. Z4080070), the Foundation of Science and Technology Bureau of Zhejiang Province, China (Grant Nos. 2008C21057 and 2009C34003), Zhejiang Province Environmental Protection Science Research Plan of China (2011B14) and the Fundamental Research Funds for the Central Universities (Program No. 2010QNA4005).

References

[1] V. Parvulescu, P. Grange, B. Delmon, Catal. Today 46 (1998) 233–316.
[2] H. Wang, J. Wang, Z. Wu, Y. Liu, Catal. Lett. 134 (2010) 295–302.
[3] J.H. Lee, S.J. Schmieg, S.H. Oh, Appl. Catal. A: Gen. 342 (2008) 78–86.
[4] M. Itoh, M. Saito, M. Takehara, K. Motoki, J. Iwamoto, K. Machida, J. Mol. Catal. A: Chem. 304 (2009) 159–165.
[5] L. Casagrande, L. Lietti, I. Nova, P. Forzatti, A. Baiker, Appl. Catal. B: Environ. 22 (1999) 63–77.
[6] Z.B. Wu, B.Q. Jiang, Y. Liu, H.Q. Wang, R.B. Jin, Environ. Sci. Technol. 41 (2007) 5812–5817.
[7] R.Q. Long, R.T. Yang, J. Catal. 194 (2000) 80–90.
[8] J.H. Li, R.H. Zhu, Y.S. Cheng, C.K. Lambert, R.T. Yang, Environ. Sci. Technol. 44 (2010) 1799–1805.
[9] B.W.L. Jang, J.J. Spivey, M.C. Kung, H.H. Kung, Energy Fuels 11 (1997) 299–306.
[10] Z. Zhu, Z. Liu, S. Liu, H. Niu, Appl. Catal. B: Environ. 30 (2001) 267–276.
[11] B. Huang, R. Huang, D. Jin, D. Ye, Catal. Today 126 (2007) 279–283.
[12] R.B. Jin, Y. Liu, Z.B. Wu, H.Q. Wang, T.T. Gu, Chemosphere 78 (2010) 1160–1166.
[13] Q. Li, H. Yang, A. Nie, X. Fan, X. Zhang, Catal. Lett (2011) 1237–1242.
[14] M.D. Amiridis, R.V. Duevel, I.E. Wachs, Appl. Catal. B: Environ. 20 (1999) 111–122.
[15] H.H. Phil, M.P. Reddy, P.A. Kumar, L.K. Ju, J.S. Hyo, Appl. Catal. B: Environ. 78 (2008) 301–308.
[16] Z.L. Liu, Y.L. Fu, J. Tu, M. Meng, Catal. Lett. 81 (2002) 285–291.
[17] B.M. Reddy, A. Khan, Y. Yamada, T. Kobayashi, S. Loridant, J.C. Volta, J. Phys. Chem. B 107 (2003) 5162–5167.
[18] L. Chen, J.H. Li, M.F. Ge, J. Phys. Chem. C 113 (2009) 21177–21184.
[19] G. Qi, R.T. Yang, J. Catal. 217 (2003) 434–441.
[20] Z.B. Wu, R.B. Jin, Y. Liu, H.Q. Wang, Catal. Commun. 9 (2008) 2217–2220.
[21] Z.B. Wu, R.B. Jin, H.Q. Wang, Y. Liu, Catal. Commun. 10 (2009) 935–939.
[22] K. Krishna, G. Seijger, C. Van den Bleek, H. Calis, Chem. Commun. 18 (2002) 2030–2031.
[23] Q. Li, H. Yang, F. Qiu, X. Zhang, J. Hazard. Mater. 192 (2011) 915–921.
[24] J.H. Goo, M.F. Irfan, S.D. Kim, S.C. Hong, Chemosphere 67 (2007) 718–723.
[25] X. Guo, C. Bartholomew, W. Hecker, L.L. Baxter, Appl. Catal. B: Environ. 92 (2009) 30–40.
[26] Z. Huang, Z. Zhu, Z. Liu, Q. Liu, J. Catal. 214 (2003) 213–219.
[27] L.A. Chen, J.H. Li, M.F. Ge, R.H. Zhu, Catal. Today 153 (2010) 77–83.
[28] S. Wang, L.J. Ji, B. Wu, Q. Gong, Y. Zhu, J. Liang, Appl. Surf. Sci. 255 (2008) 3263–3266.
[29] J.H. Li, J.J. Chen, R. Ke, C.K. Luo, J.M. Hao, Catal. Commun. 8 (2007) 1896–1900.
[30] S. Lefrant, M. Baibarac, I. Baltog, J. Mater. Chem. 19 (2009) 5690–5704.
[31] J.A. Martin, M. Yates, P. Avila, S. Suarez, J. Blanco, Appl. Catal. B: Environ. 70 (2007) 330–334.
[32] M. Kang, E.D. Park, J.M. Kim, J.E. Yie, Appl. Catal. A: Gen. 327 (2007) 261–269.
[33] B. Fleutot, H. Martinez, B. Pecquenard, J.B. Ledeuil, A. Levasseur, D. Gonbeau, J. Power Sources 180 (2008) 836–844.
[34] Q. Zhong, Y.T. Li, J. Hazard. Mater. 172 (2009) 635–640.
[35] L.A. Chen, J.H. Li, M.F. Ge, Environ. Sci. Technol. 44 (2010) 9590–9596.
[36] W. Tian, H. Yang, X. Fan, X. Zhang, J. Hazard. Mater. 188 (2011) 105–109.
[37] M. Reiche, E. Ortelli, A. Baiker, Appl. Catal. B: Environ. 23 (1999) 187–203.
[38] S. Xu, X. Wang, Fuel 84 (2005) 563–567.